Unusual semimetallic behavior of carbonized ion-implanted polymers

G. Du*
Department of Physics, The Ohio State University, Columbus, Ohio 43210-1106

V. N. Prigodin
Department of Physics, The Ohio State University, Columbus, Ohio 43210-1106
and A. F. Ioffe Physico-Technical Institute, 194021 St. Petersburg, Russia

A. Burns† and J. Joo‡
Department of Physics, The Ohio State University, Columbus, Ohio 43210-1106

C. S. Wang
University of Dayton Research Institute, Dayton, Ohio 45469

A. J. Epstein
Department of Physics, The Ohio State University, Columbus, Ohio 43210-1106
(Received 16 December 1997)

We report a comprehensive charge transport study of ion-implanted rigid rod and ladder polymers *p*-phenylenebenzobisoxazole, *p*-phenylenebenzobisthiazole, and benzimidazobenzophenanthroline. The three pristine materials are strong and stable polymers with a room temperature conductivity $\sigma_{RT}\sim 10^{-12}$ S/cm. After high dosage ion implantation using Kr^+, a carbonized and conducting layer forms on the surface of the film samples with $\sigma_{RT}>10^2$ S/cm. The experimental results suggest that this carbonized layer is semimetallic with unusual properties. The observed dc conductivity follows $\sigma(T)=\sigma_0+\Delta\sigma(T)$, where $\Delta\sigma(T)$ is weakly temperature dependent and interpreted within the model of weak localization and electron-electron interaction effects. The model reveals that the interaction effect is three dimensional for the experimental temperature range (3–300 K), whereas the weak localization effect undergoes a dimensional crossover at ~60 K from three to two-dimensions with decreasing temperature. The magnetoconductance, thermoelectric power, and microwave dielectric constant results are all in agreement with this semimetallic model. In addition, all these results consistently point to an enhanced interaction effect at low temperatures due to the reduced dimensionality of the localization effect. It is concluded that a sp^2 rich and three-dimensional interconnected carbon network reformed upon ion implantation of the densely packed pristine polymers is responsible for the semimetallic behavior. [S0163-1829(98)09231-5]

I. INTRODUCTION

Ion implantation is a well known industrial technique for modifying the electronic properties of semiconductors.[1,2] Some insulating polymers treated by this process also have shown a change in their electronic properties, among which was a very large increase in the room temperature conductivity σ_{RT} from $\sim 10^{-12}$ to $>10^2$ S/cm after ion irradiation.[1–3] A general insulating conductivity

$$\sigma(T)\propto\exp[-(T_0/T)^{\gamma}] \tag{1}$$

seems to be a common result from these earlier reports.[2–4] Apparently, a disorder induced Anderson insulator-metal transition is in progress in these systems upon ion implantation. However, none of these earlier studies observed a true metallic phase in the systems studied as the temperature dependence of the observed conductivity usually following Eq. (1) is not metallic.[1,2] A value of $\gamma\cong 0.5$ was frequently observed and interpreted in terms of either quasi-one-dimensional variable range hopping[2] or tunneling between metallic particles embedded in an insulating medium.[3] The difficulty in sorting out these results lies in the complex morphology of these implanted polymers. The ion irradiation interrupts the original polymer structure by scissoring covalent bonds and driving heteroatoms out of the system (detected by the outgassing of various gases during the implantation).[2] The extent of this interruption depends on several factors including the type and energy of the ions, but primarily on the implantation dosage level. At high dosages, the implanted system becomes highly amorphous. Experimental results from x-ray diffraction, Raman scattering, and x-ray photoelectron spectroscopy also suggest that the irradiated samples are highly carbonized.[2,5,6] Therefore, one actually obtains a conducting layer of amorphous carbons in ion implanted polymers.

It has been known that carbonaceous materials have a wide range of transport properties from insulating diamond to metallic graphite. In between these two opposite crystalline forms of carbons, various amorphous carbons have shown conduction states covering the whole conduction spectrum from the insulating end to the metallic end depending upon the type (sp^2 or sp^3) and order of C-C bonds of these systems.[7] Hence the structure and composition of the reformed carbon networks in these implanted polymers are

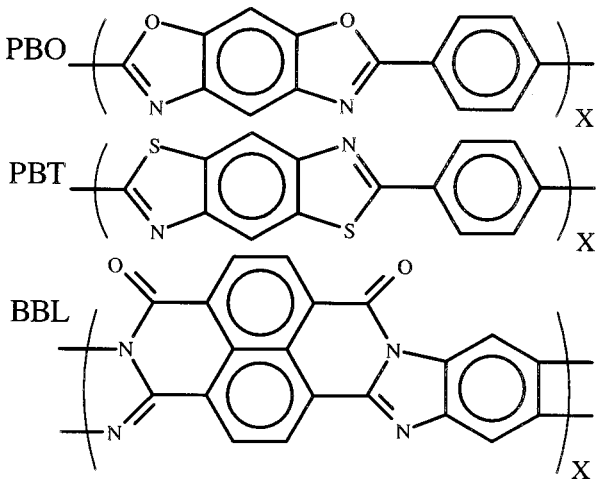

FIG. 1. Pristine structure of PBO, PBT, and BBL polymers.

essential in determining their conduction properties. In other words, whether a reformed carbon network is 2D/3D interconnected or resumes more or less the original polymeric 1D chain-like structure and whether sp^2 or sp^3 bonding dominates are the factors determining its transport properties. On the other hand, these two aspects of a reformed carbon network are closely related to the pristine polymer backbone structure that serves as a base for the reformed carbon network after ion implantation.

In this paper we report a comprehensive transport study of ion-implanted *p*-phenylenebenzobisoxazole (PBO), *p*-phenylenebenzobisthiazole (PBT), and benzimidazobenzophenanthroline (BBL) polymers. The three pristine materials are strong and stable polymers with their polymer chains densely packed on the microscopic level, which is a key difference from other polymers used in the earlier studies.[2,3] PBO and PBT are rigid rod polymers and BBL is a ladder polymer so named because of the two covalent bonds between repeating units (Fig. 1). These pristine polymers have a room temperature conductivity $\sigma_{RT} \sim 10^{-12}$ S/cm. After implantation using high-energy Kr^+ ions at a high dosage, their σ_{RT} increases about 14 orders to $>10^2$ S/cm. Yet the most drastic result from this study is the temperature dependence of the conductivity. Instead of the normally observed hopping or tunneling conductivity [Eq. (1)] of the earlier ion implanted polymers, these implanted rigid-rod and ladder polymers have a very weak temperature-dependent conductivity. The conductivity data fit best to a semimetallic model $\sigma(T)=\sigma_0+\Delta\sigma(T)$, where the temperature dependent correction term $\Delta\sigma(T)$ is due to the electron-electron interaction and weak localization effects.[8,9] Through the fitting parameters obtained from the conductivity data, this model reveals that the electron-electron interaction contribution is three dimensional over the experimental temperature range 3–300 K. However, the weak localization correction effect, additive to the interaction correction effect, is found to experience a dimensional transition from three dimensions at temperatures above ~60 K to two dimensions at lower temperatures. The extrapolated zero-temperature conductivity $\sigma(T\rightarrow 0)$ of these samples is smaller than that usually observed in disorder metals as well as 3D Mott's minimum metallic conductivity; however, it is within the scope of the more recent scaling theory in which the minimum metallic conductivity is zero.[8,9] As a comparison, we also studied low-dosage implanted PBO samples. These systems exhibited an insulating hopping conductivity instead of the metallic one presented in this paper. Obviously, the low-dosage samples are on the insulating side of an insulator-metal transition controlled by ion implantation dosage.[10]

The combination of interaction and localization effects are more clearly revealed in the magnetoconductance results. At $T>30$ K, magnetoconductance $\Delta\sigma(H,T)$ is positive, typically observed in disordered metals or doped semiconductors with a dominant weak localization effect.[8,9] At lower temperatures, the magnetoconductance data changed sign from positive to negative, apparently due to an enhanced and dominant interaction effect. This change of dominance from localization effect to interaction effect with decreasing temperature results from a reduction in dimensionality of the localization effect at low temperatures. The thermoelectric power data are linear with temperature at higher temperatures, which is usual for a metallic system. The low-temperature thermopower data deviate from this linear temperature dependence and change to a $1/T$ dependence. This unusual change in thermopower data is also explained in terms of the enhanced electron-electron interaction effect, which causes a depletion in the density of states at the Fermi level at low temperatures.[11] The microwave dielectric constant results of these systems are positive and large ($\sim 10^4$) over the whole temperature range, also consistent with the weak localization model.[2,12] The low-temperature dielectric constant ($T<40$ K), decreasing more rapidly with temperature due to the decreasing density of states at the Fermi level, provides yet another piece of evidence for the enhanced interaction effect in this temperature region. Therefore, all these experimental results consistently demonstrate that these implanted polymers are on the metallic side of the Anderson transition with a unusual low-temperature phase characterized by an enhanced electron-electron interaction effect due to a reduced dimensionality of the localization effect. The difference between these implanted polymers and the ones studied earlier[2,3] is the pristine structure of these rigid-rod and ladder polymers that provides a microscopically compact carbon backbone for the reformed 3D interconnected and sp^2 rich carbon network responsible for the semimetallic behavior.

II. EXPERIMENT

The pristine PBO, PBT, and BBL polymers were obtained in the form of aggregated films, free standing and about 50 μm thick (supplied by the Polymer Branch, Materials Directorate, Air Force Research Laboratory, Dayton, OH). The synthesis and processing of these polymers were published previously.[13] The implantation was performed by a Varian 400-AR ion implantor at Honeywell Systems and Research Center, Minneapolis, MN, using 200 KeV $^{84}Kr^+$ ions at an ion beam current density of $2\mu A/cm^2$ and ion dosage of 4×10^{16} ions/cm^2. The implantation[6] creates a conducting layer [$\sim 0.1-0.2$ μm thick, estimated from scanning electron microscopy (SEM)] on the surface of all three film samples. The dc conductivity and magnetoconductance measurements utilized a conventional four-probe planar sample configuration with gold wires and silver paint

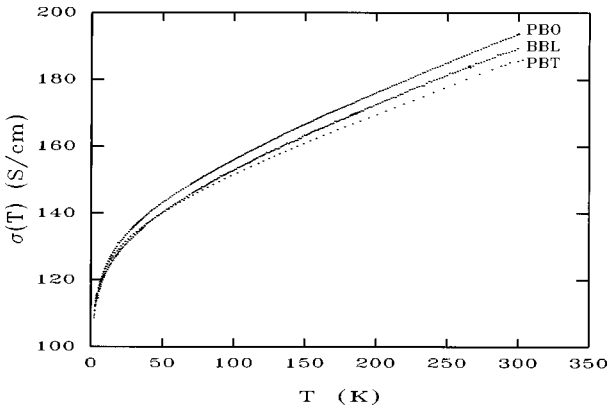

FIG. 2. dc conductivity results $\sigma(T)$ of the implanted PBO, PBT, and BBL polymers.

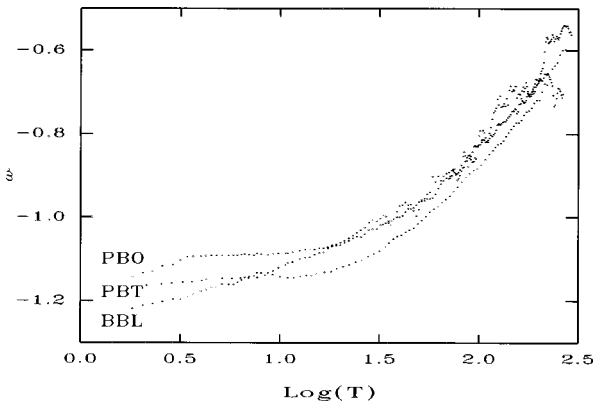

FIG. 3. w plot of the implanted PBO, PBT, and BBL polymers.

used and the data were taken from a computer controlled current source (Keithley 220) and a multimeter (Keithley 195A). The magnetic field up to 7.5 T was provided by a Janis Supervaritemp Dewar flask. The temperature in these experiments was controlled from 3 to 300 K using liquid helium in the Janis Dewar flask by a LakeShore DRC 82C Temperature Controller and LakeShore DT500 thermosensors. The microwave dielectric constant was measured by a cavity perturbation technique[14] using a homemade cavity (TM_{010} mode at 6.5 GHz) with the microwave source provided by a Hewlett-Pachard 8350B Sweep Generator. Thermoelectric power experiment used a sample holder similar to that of Ref. 15 and the data were recorded by two Keithley 180 nanvoltmeters and a Hewlett-Packard 7004B X-Y recorder. A standard copper-tungsten thermocouple was used to measure the temperature gradient across the sample achieved by heating one of the two sample mounting quartz blocks wrapped with heating wires using a Keithley 220 current source. The temperature control for these two experiments is similar to that of the conductivity experiments.

III. RESULTS AND ANALYSIS

A. dc conductivity

1. Conductivity and the w plot

Figure 2 plots the temperature-dependent dc conductivity results of the three implanted polymers. A sample thickness of $t=0.15\ \mu$m estimated from a measurement of 0.1–0.2 $<\mu$m by SEM was used to calculate all conductivity data. The three sets of data are very similar in magnitude and temperature dependence. The difference between the three results, $<5\%$, is well within the experimental errors in the sample dimension measurements. The similarity between the electronic properties of these three implanted polymers suggests that the conducting carbonized layers formed from three different pristine polymers are similar as far as the type and order of C-C bonds are concerned.

These weakly temperature-dependent conductivity data have a conductivity ratio, $\sigma_{RT}/\sigma(4\ \mathrm{K})$ less than a factor of 2 for all three materials. In order to reveal the exact temperature dependence of the conductivity, a procedure employed by Ref. 16 is used, which is to plot the quantity

$$w(T)=\log_{10}\left(\frac{d\{\ln[\sigma(T)]\}}{d[\ln(T)]}\right) \tag{2}$$

versus $\log_{10}(T)$. For an insulating conductivity with the general form of Eq. (1), the w plot yields a straight line with a negative slope $-\gamma$ ($\gamma>0$). For example, the activation type of conduction of semiconductors would give rise to $\gamma=1$ and Mott's variable range hopping conduction to $\gamma=1/(1+d)$, where d is the dimensionality of the sample concerned.[17] For disordered metals or doped semiconductors, a semimetallic behavior $\sigma(T)=\sigma_0+\Delta\sigma(T)$ has been commonly observed.[8,9,18,19] The w plot of such a temperature-dependent conductivity yields a curve with a positive slope.

Figure 3 shows the w plots of the three samples. None of the curves possesses a negative slope over the whole temperature range. In other words, these w plots exclude the general hopping or tunneling conduction mechanism Eq. (1) for these implanted polymers. In addition, the fitting of the conductivity data to a weak localization and electron-electron interaction model to be discussed in Sec. III A 3 yields a nonzero conductivity at zero temperature (Drude conductivity σ_0) for these systems. The w plot and nonzero σ_0 results together provide direct evidence that these three implanted polymers, in the form of reformed carbon networks, are on the metallic side of an insulator-metal transition. Hence these implanted polymers are qualitatively and quantitatively different from the previously studied implanted polymers that have a zero conductivity at zero temperature and are obviously on the insulating side of an insulator-metal transition.[2,3]

2. Scaling theory of localization and the Coulomb interaction model

Numerous experimental studies of disordered metals such as alloys and doped semiconductors suggest that a scaling theory of localization and electron-electron interaction is universal in describing various disordered metallic systems.[8,9] This model predicts that in such a semimetallic system the temperature dependent correction terms, arising from localization (L) and interaction (I) effects, are additive to the Drude conductivity σ_0 in the lowest order,

$$\sigma(T)=\sigma_0+\Delta\sigma_L(T)+\Delta\sigma_I(T). \tag{3}$$

TABLE I. Fitting functions applied to the implanted PBO conductivity data and the corresponding fitting errors [Eq. (8)] for three different temperature ranges: 3–300 K, 3–30 K, and 30–300 K.

$\sigma(T)$	Errors (3–300 K)	Errors (3–30 K)	Errors (30–300 K)
$\sigma_0+B\ln(T)$	27.4	4.58×10^{-2}	11.0
$\sigma_0+mT^{1/2}$	0.827	0.449	0.61
$\sigma_0+mT^{1/2}+B\ln(T)$	0.826	2.30×10^{-2}	8.60×10^{-2}
$\sigma_0+mT^{1/2}+BT^{3/2}$	0.687	5.19×10^{-2}	1.07×10^{-2}

The localization correction term due to coherent backscattering processes in between dephasing inelastic scattering events, characterized by the Thouless length L_{Th}, is given by[8,9]

$$\Delta\sigma_L^{3D}(T)=\frac{e^2}{2\pi^2\hbar L_{Th}}=\frac{e^2}{2a\pi^2\hbar}T^{p/2}, \tag{4}$$

$$\Delta\sigma_L^{2D}(T)=\frac{e^2}{2\pi^2\hbar}\ln\left(\frac{1}{L_{Th}}\right)=\frac{\alpha p e^2}{2\pi^2\hbar}\ln(T) \tag{5}$$

for the 3D and 2D cases, respectively, where a and α are fitting parameters. The value of α should be close to 1.[9] The Thouless length is given by $L_{Th}=(D\tau_{in})^{1/2}$, where D is diffusion constant and $\tau_{in}\propto T^{-p}$, $p>1$, is the inelastic scattering time.[8,9] The Thouless length is used to determine the dimensionality of a sample. For an electronically thick or 3D system, the Thouless length should be less than the sample thickness, i.e., $L_{Th}<t$; but if $t<L_{Th}$, the sample is electronically thin and 2D for the localization effect.[9] It should be noted that factor p makes a difference in the temperature dependence of the weak localization effect $T^{p/2}$ [Eq. (4)] for a 3D case; for 2D systems, the temperature dependence $\ln(T)$ [Eq. (5)] is always the same. The values of p are given by this theory at 3/2, 2, and 3,[9] depending on whether electron-electron scattering in the dirty limit (characterized by $T<\tau_0^{-1}$ where τ_0 is the elastic scattering time), clean limit ($T>\tau_0^{-1}$), or electron-phonon scattering dominates the inelastic scattering rate, respectively.[9]

The interaction correction term to the Drude conductivity σ_0 for a 3D case is given by

$$\Delta\sigma_I^{3d}(T)=\frac{e^2}{4\pi^2\hbar}\frac{1.3}{\sqrt{2}}\left(\frac{4}{3}-\frac{3}{2}F\right)\sqrt{\frac{k_BT}{\hbar D}}, \tag{6}$$

where F is electron screening factor.[9] In the presence of a strong electron screening such as in metals, $F\cong1$, while for little or no screening such as in strongly localized systems, $F\cong0$.[8] The Coulomb interaction effect has a different characteristic length $L_c=(\hbar D/k_BT)^{1/2}$ for judging its dimensionality in a sample.[9] That is, if $L_c<t$, it is 3D and if $L_c>t$, it is 2D for this effect.

3. Fitting of the dc conductivity data

From the shape of the weak temperature dependence of the conductivity data (Fig. 2), it is very suggestive to fit the data to functions

$$\sigma(T)=\sigma_0+AT^{\beta} \quad \text{or} \quad \sigma(T)=\sigma_0+A\ln(T). \tag{7}$$

These two temperature dependences have been reported in many disordered metallic systems.[8,9] However, these functions do not fit the data of these implanted polymers well over the whole temperature range. Using the implanted PBO conductivity data as an example of various fittings, Table I lists some related and meaningful fitting functions with their corresponding fitting errors. The fitting error is given by

$$N^{-1}\sum_{i=1}^{N}[\sigma_i-\sigma(T)]^2, \tag{8}$$

where N is the number of data points and σ_i is the ith measured conductivity at T. The addition of one more temperature-dependent term to Eq. (7) not only is desirable to lower the fitting error but also stays within the theoretical understanding of weak localization and electron-electron interaction.[18–20] As shown in Table I, the two correction term functions generally lower the fitting errors over those with just one correction term. However, further fitting analysis shows that the two correction term functions work better in either of the two subtemperature regions 3–30 K or 30–300 K than in the whole temperature range 3–300 K. As one can see from Table I, function (3) fits the data best at lower temperatures (3–30 K), while function (4) fits best at higher temperatures (30–300 K). The fitting of the implanted PBT and BBL data yields similar results.

The above fitting analysis eventually leads us to the following model, which fits the observed conductivity data almost perfectly over the whole temperature range:[21]

$$\sigma(T)=\sigma_0+mT^{1/2}+B\ln[\sinh(T/c)^{3/2}], \tag{9}$$

where σ_0, c, m, and B are fitting parameters. Table II lists these parameters and the fitting errors for fittings from 3 to 300 K for the three implanted polymers. Figure 4 plots the conductivity data of the implanted PBO and the fitting function of Eq. (9), using the parameters from Table II, showing an excellent match.

When $T\gg c$, Eq. (9) becomes

$$\sigma(T)=\sigma_0'+mT^{1/2}+B'T^{3/2}, \tag{10}$$

where $\sigma_0'=\sigma_0-B\ln(2)$ and $B'=Bc^{-3/2}$. When $T\ll c$, one obtains the low-temperature asymptote

$$\sigma(T)=\sigma_0''+mT^{1/2}+1.5B\ln(T), \tag{11}$$

where $\sigma_0''=\sigma_0-1.5B\ln(c)$.

TABLE II. Fitting parameters σ_0, m, B, and c of Eq. (9) for the implanted PBO, PBT, and BBL conductivity data (from 3 to 300 K). The last two columns are calculated at 300 K.

Sample	σ_0 (S/cm)	m (S/cm K$^{1/2}$)	B (S/cm)	c (K)	Error	$mT^{1/2}/\sigma_0'$	$B'T^{3/2}/\sigma_0'$
PBO	113	4.15	0.787	59	0.43	0.64	0.075
PBT	112	3.84	0.725	56	2.43	0.60	0.076
BBL	111	4.05	0.722	57	0.15	0.63	0.074

Equation (10) suggests that at high temperatures the electron conduction is characterized by a weak localization effect [the $T^{3/2}$ term, comparable to Eq. (4)] and an interaction effect [the $T^{1/2}$ term, matching Eq. (6)] in addition to the Drude conductivity with both effects in a 3D case. By comparing $T^{3/2}$ with $T^{p/2}$ of Eq. (4) for a 3D weak localization effect, one obtains $p=3$, which indicates that electron-phonon scattering dominates inelastic scattering in these materials (see Sec. III A 2). Similarly, Eq. (11) suggests that at low temperatures the weak localization effect [the ln(T) term, matching Eq. (5)] is 2D, while the interaction effect (the $T^{1/2}$ term) is still 3D. Therefore, the fitting of Eq. (9) from 3 to 300 K reveals that the weak localization effect changes its dimensionality from 2D to 3D with increasing temperature, while the interaction effect remains 3D throughout the whole temperature range. A detailed analysis of this dimensional transition will be given in Sec. III A 4.

By comparing the fitting parameter m of the $T^{1/2}$ term in Eq. (9) (given in Table II) with the coefficient of Eq. (6),

$$\frac{e^2}{4\pi^2\hbar}\frac{1.3}{\sqrt{2}}\left(\frac{4}{3}-\frac{3}{2}F\right)\sqrt{\frac{k_B}{\hbar D}}=m, \tag{12}$$

one obtains the upper limit for diffusion constant D (listed in Table III), assuming a bare electron screening case, i.e., $F \cong 0$, in these amorphous systems (see the discussion in Sec. III A 7 below). From the value of D, one can calculate the Coulomb interaction characteristic length $L_c=(\hbar D/k_BT)^{1/2}$ (upper limit). The L_c values of the three materials at 3 K are also listed in Table III.

In a similar manner, by comparing the $B'T^{3/2}$ term of Eq. (10) ($B'=Bc^{-3/2}$, B, and c from Table II) with Eq. (4) and by comparing the coefficient of the ln(T) term of Eq. (11) (1.5B and B from Table II) with that of Eq. (5), respectively,

$$\frac{e^2}{2\pi^2\hbar L_{Th}}=Bc^{-3/2}T^{3/2}, \tag{13}$$

$$\frac{\alpha p e^2}{2\pi^2\hbar}=1.5B \quad (p=3), \tag{14}$$

one obtains the Thouless length L_{Th} and factor α. Similar fitting results are obtained for the three implanted polymers and are listed in Table III.

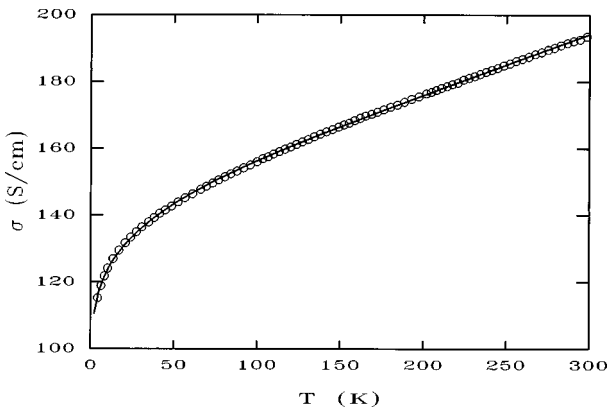

FIG. 4. dc conductivity of implanted PBO (circles) and fitting function (9) using parameters from Table II (solid lines).

4. Validity of the model

The fitting parameters obtained in the preceding subsection allow us to verify this model as well as look into the physics governing these materials. For the fitting results to make sense according to the theory,[9] the localization [the $T^{3/2}$ or ln(T) term] and interaction (the $T^{1/2}$ term) effects should be first-order corrections to the Drude conductivity in the concerned temperature range. As shown in Table II, these two effects are indeed approximately first-order corrections to the zero-temperature conductivity up to room temperature. Here only the 3D case of the localization effect is tested since the 2D case exists only at low temperatures. Another direct fitting result, the parameter α in Eq. (5), turns out to be very close to unity (Table III) just as predicted by the theory.[9]

As suggested by the $T^{1/2}$ terms in Eqs. (10) and (11), the Coulomb interaction effect is 3D over the whole temperature range 3–300 K. According to the theory,[9] the interaction characteristic length $L_c=(\hbar D/k_BT)^{1/2}$ should be shorter than the sample thickness t for a 3D system. Using the diffusion constant D from Table III, a short $L_c \sim 110$ Å, is obtained even at 3 K. This length is more than one order of magnitude

TABLE III. Values of L_{Th}, T_s, D_m, L_c, and α obtained from the fitting parameters of Table II. T_s is the temperature at which the Thouless length L_{Th} equals the sample thickness. D_m is the upper limit for the diffusion constant, assuming the screening factor $F=0$. $L_c=(\hbar D_m/k_BT)^{1/2}$ is calculated at 3 K.

Sample	L_{Th} (m)	T_s (K)	D_m (cm^2/s)	L_c (3 K) (Å)	α
PBO	$7.1\times10^{-5}T^{-3/2}$	60.7	0.43	105	1.11
PBT	$7.1\times10^{-5}T^{-3/2}$	60.9	0.51	113	1.03
BBL	$7.3\times10^{-5}T^{-3/2}$	62.1	0.46	108	1.03

shorter than the sample thickness t (~1500 Å) of these samples. At higher temperatures, L_c is even shorter; thus the interaction effect should be 3D from 3 K and above.

According to the weak localization theory, the power p dictating the temperature dependence of the Thouless length $L_{Th} \propto T^{-p/2}$ is determined by the nature of dominant inelastic scattering process.[9] For example, Refs. 18 and 22 reported cases of $p=2$ for doped semiconductors, suggesting electron-electron scattering in the clean limit as the dominant inelastic scattering for these systems. Other values of $p>1$ have also been reported for a variety of disordered metallic systems.[19,20] The fitting of Eq. (9), working best with $p=3$ for these implanted materials, suggests that electron-phonon scattering determines the inelastic scattering rate in these systems. This result is consistent with the amorphous nature of the reformed carbon network of these implanted polymers. In such a highly disordered system, one would expect electron-phonon scattering dominating electron-electron scattering. More discussion on this point will be given in Sec. III A 6.

The dimensionality of the weak localization effect is determined by comparing the Thouless length L_{Th} (Table III) with sample thickness t. Taking implanted PBO as an example, at

$$L_{Th} = 7.1 \times 10^{-5} T^{-3/2} = t, \tag{15}$$

one can calculate the temperature $T=T_s$ that separates the 2D phase from the 3D phase. As shown in Table III, $T_s \cong 60$ K is obtained for all three implanted polymers. For $T > T_s$, one has $L_{th} < t$ and the system is 3D for the localization effect; for $T < T_s$, the system is 2D for this effect, satisfying the condition $L_{Th} > t$. The fact that the value of T_s matches the fitting parameter c of Eq. (9) (Table II) very well for all three samples shows that this model is self-consistent. However, it should be noted that the Thouless length or inelastic scattering time obtained from these implanted polymers is larger than that of doped semiconductors or disordered metals.[18–20,22,23] This difference can be explained by the fact that in all those cases, the inelastic scattering rate is dominated by electron-electron scattering in either the dirty (yielding $p=3/2$) or clean (yielding $p=2$) limit, whereas in these implanted rigid-rod and ladder polymers electron-phonon scattering dominates the inelastic scattering rate (yielding $p=3$).

5. Mott's minimum metallic conductivity

The dc conductivity results presented above and other experimental results (to be presented below) all suggest these carbonized systems are on the metallic side of an insulator-metal transition. However, the zero-temperature conductivity of these implanted polymers, ~110 S/cm (calculated at thickness $t=0.15$ μm, or ~80–160 S/cm for t between 0.2–0.1 μm), is considered only moderate as compared to that of disordered metals, $\sim 10^3$–10^4 S/cm, even though they exhibit a similar semimetallic behavior.[8,9] The Mott minimum metallic conductivities in 3D and 2D cases are given by[9,17]

$$\sigma_{min}^{3D} = c' \frac{e^2}{\hbar a_0}, \tag{16}$$

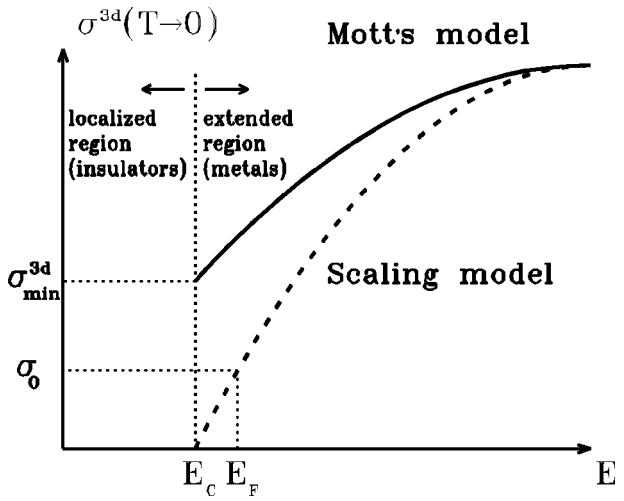

FIG. 5. Continuous (broken line) and discontinuous (solid line) metal-insulator transition models of the minimun metallic conductivity. E_c is the mobility edge separating the localized region or insulators from the extended region or metals.

$$\sigma_{min}^{2D} = c'' \frac{e^2}{\hbar}, \tag{17}$$

respectively, where a_0 is the microscopic length scale in the problem and coefficient c' varies slightly according to different authors.[17,24] Reference 24 obtained universal values for $c' = 0.07 \pm 0.01$ and $c'' = 0.11 \pm 0.02$. From a 3D point of view, using $c' = 0.07$ and a typical sp^2 C-C bond length $a_0 = 1.4$ Å, $\sigma_{min}^{3D} \sim 1.3 \times 10^3$ S/cm is obtained, which is much larger than the observed zero-temperature conductivity. From a 2D point of view, Eq. (17) yields $\sigma_{min}^{2D} = 2.4 \times 10^{-5}$ S, which is sample dimension independent. The observed 2D zero-temperature conductivity is given by $\sim 110 \times t \cong 1.7 \times 10^{-3}$ S, which is larger than the predicted σ_{min}^{2D}.

The above comparison between the minimum metallic conductivity with the observed value in the 3D case seems in violation of Mott's metal-insulator transition model in which the mobility edge E_C marks the transition with $\sigma^{3D}(T\to 0)$ changing from σ_{min}^{3D} to zero abruptly (Fig. 5).[17] However, the more recent scaling theory of localization predicts $\sigma^{3D}(T \to 0) \propto (E - E_C)^{\mu}$.[9,19] Thus the insulator-metal transition is continuous in $\sigma^{3D}(T\to 0)$ from the scaling theory point of view rather than discontinuous as predicted by the Mott model. In other words, any finite conductivity at zero temperature indicates a metallic system according to the scaling theory. Figure 5 illustrates these two different models. The earlier studies on insulator-metal transition in doped semiconductors have reported similar finite zero-temperature conductivities, smaller than the Mott minimum metallic value.[8,18,19]

6. Conduction electrons and the reformed carbon network

The above analysis of the conductivity results leads to several conclusions. The smaller $\sigma^{3D}(T\to 0)$ indicates that these carbonized systems are just over the insulator-metal transition boundary into the metallic side. In other words, the Fermi energy E_F just passes the mobility edge E_C and locates in the extended state region (Fig. 5). As a result, these

systems have fewer extended electrons, or a smaller conduction electron density, than the more metallic systems. This conclusion is consistent with the fitting result of $p=3$, indicating electron-phonon scattering dominating the inelastic scattering rate in these materials. As mentioned earlier, values of p other than 3 have been reported for more metallic systems, which indicates dominant electron-electron scattering in these systems.[18–20,22] For a highly disordered system with a small free-electron population, electron-phonon scattering is more likely to occur than electron-electron scattering.

However, where do these extended electrons come from in the implanted polymers? Dresselhaus and co-workers[2] proposed that the ion bombardment results in breaking of various bonds and scission of polymers chains and creates free radicals and charged centers along the original polymer backbone. A concentration of charged carriers must be generated simultaneously to maintain the charge neutrality and give rise to the electron conductivity. However, these charge carriers are most likely to be strongly localized [as mentioned above, their reports showed the insulating hopping conductivity of Eq. (1)]. The free-electron gas in implanted PBO, PBT, and BBL must form from a different route. Recall that ion implantation expels heteroatoms out of the samples, for example, N and O atoms from PBO. As a result, a system containing mostly carbon reforms after the implantation process, with new C-C bonds forming in either sp^2 or sp^3 hybridized orbitals. The large number of unsaturated bonds in the three pristine polymers (Fig. 1) dictates that the reformed carbon network is likely sp^2 dominant. It is these sp^2 carbons with their unpaired π electrons that contribute to a free-electron gas in these implanted materials.

However, for these systems to be metallic, these electrons have to be able to extend over the whole sample. We propose a scenario that quasiplanar patches of graphitelike structures from sp^2 carbons form in these implanted systems and are interrupted three dimensionally by the randomly distributed sp^3 sites. The overlap between the adjacent extended wave functions from the neighboring graphitelike structures is strong enough for the delocalized π electrons to percolate through the entire sample. When the Thouless length is smaller than the sample thickness, this 3D interconnected carbon network is electronically thick or 3D electronically, while as the Thouless length increases with decreasing temperature and surpasses the sample thickness, the implanted layer becomes 2D electronically even though the structure is 3D in nature.

The factors in determining the electronic properties of the implanted polymers are several fold. First is the ion implantation process, which includes the type of ions, its energy, and implantation dosage.[10] The second factor that may cause a difference is the chemical composition of a polymer. The amount and type of heteroatoms and number of unsaturated bonds in a polymer will affect the formation of the reformed carbon network and its electronic properties. Finally is the packing compactness of the pristine polymer chains in the samples. Polymers PBO, PBT, and BBL, well known for their superior stability and mechanical properties,[13] are very densely packed samples with a partial local order. For instance, x-ray studies show that polymer PBT has a packing order, or distance between adjacent cofacial polymer chains, ~ 3.54 Å (Ref. 25) and BBL ~ 3.37 Å.[26] Highly disordered amorphous polymer films, such as the ones used in the earlier ion implantation studies, lack such local order and dense packing of the polymer chains. This dense packing provides a foundation for the 3D interconnected carbon network after implantation. The similar electronic properties of these three implanted polymers suggest that they have similar final reformed carbon networks probably resulting from similarly packed pristine polymers. For the loosely packed polymer samples, the reformed carbon network after implantation likely resumes the 1D chainlike structure of the original polymers. The conduction state of these systems will not be as metallic as the 3D structures. This analysis can account for the difference between implanted PBO, PBT, and BBL and the earlier implanted polymers. In many of the earlier reports, Mott's 1D variable range hopping model was found to fit the experimental results well.[2,4]

7. Long-range Coulomb interactions

It has not escaped our notice that the Coulomb interaction effect manifests in the conductivity results of these implanted systems at room temperature and maybe higher. A similar interaction effect has been observed in many disordered metallic systems, usually below 100 K or at much lower temperatures.[8,27] This difference can be explained by the relative extent of disorder and degree of electron screening of a material. In the more metallic systems such as disordered metals and doped semiconductors, the Fermi level is deep into the extended region with a larger free-electron density and the localization effect due to disorder is not as strong as in the highly amorphous systems. Under this circumstance, the electron screening is strong [$F\cong 1$ in Eq. (6)]. Therefore, in order to observe the interaction effect, one has to reach lower temperatures. For the more amorphous systems on the other hand, it is the opposite situation. The stronger localization and smaller conduction charge density lead to a weak electron screening ($F\cong 0$). Thus the interaction effect is not as suppressed at higher temperatures as it is in the more metallic systems.

B. Magnetoconductance

Magnetotransport has been a very useful experimental tool to probe the localization and interaction effects in conducting materials.[8,9] In this experiment, the measured quantity is actually the resistivity tensor ρ_{xx}, which is related to the conductivity by

$$\rho_{xx}=\frac{\sigma_{xx}}{\sigma_{xx}^2+\sigma_{xy}^2}, \tag{18}$$

where σ_{xx} is the quantity to be compared with theory and $\sigma_{xy}=R_H H\sigma_{xx}/(1-\sigma_{xy})$ is the Hall conductivity, in which R_H is the Hall coefficient.[28] A measurement of Hall coefficient was conducted at 4.2 K. The exact Hall signal was not obtained due to a large noise-to-signal ratio. However, the upper limit of the Hall coefficient can be estimated at 10^{-8} Ω m/T with an applied magnetic field $H=7.5$ T. Using $\sigma_{xx}\cong\sigma_{dc}\cong 50$ S/cm, one obtains $\sigma_{xy}\leqslant 10^{-3}$ S/cm, which is much smaller than σ_{xx}. Thus σ_{xy} can be neglected in Eq. (18), which yields $\sigma_{xx}=1/\rho_{xx}$.

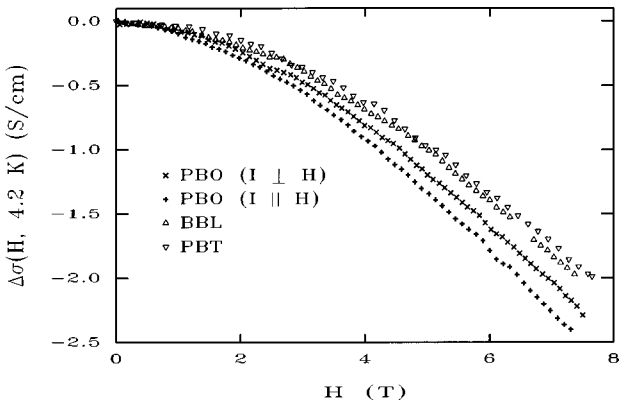

FIG. 6. Magnetoconductance of the implanted PBO, PBT, and BBL at 4.2 K.

Magnetoconductance results $\Delta\sigma(H,T)=\sigma_{xx}(H,T)-\sigma_{xx}(0,T)$ of the three samples were obtained at several temperatures between 2 and 40 K as a function of the applied magnetic field H (up to 7.5 T). No significant magnetoconductance could be observed at higher temperatures. Figure 6 plots the magnetoconductance results of the three implanted polymers at 4.2 K. As one can see, the three samples have similar magnetoconductance results. In addition, the magnetoconductance data measured at field perpendicular to the current ($H\perp I$) and at field parallel to the current ($H\|I$) are almost identical. These two measurement results of the implanted PBO are also shown in Fig. 6. The similar magnetoconductance for the three samples again suggests that the reformed carbon network is similar in the three samples after implantation. Figure 7 plots the magnetoconductance results of the implanted PBO at different temperatures. As one can see, the magnetoconductance changes sign from negative at lower temperatures ($\lesssim$30K) to positive at higher temperatures ($\gtrsim$30K).

This change of sign of the magnetoconductance results can be explained using the same model of Sec. III A 3. From the discussion of the conductivity fitting, we conclude that the weak localization effect is 2D at low temperatures and the interaction effect is 3D over the whole temperature range 3–300 K. Thus, in the low-temperature region,

$$\Delta\sigma(H,T)=\Delta\sigma_L^{2D}(H,T)+\Delta\sigma_I^{3D}(H,T). \tag{19}$$

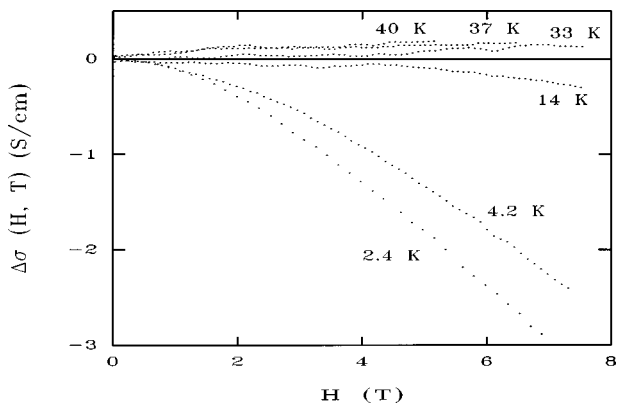

FIG. 7. Magnetoconductance of the implanted PBO at different temperatures.

At higher temperatures, the magnetoconductance should be

$$\Delta\sigma(H,T)=\Delta\sigma_L^{3D}(H,T)+\Delta\sigma_I^{3D}(H,T). \tag{20}$$

In the presence of an external magnetic field, the phase coherence in backscattering of the weakly localized regime is destroyed, leading to a negative magnetoresistance or positive magnetoconductance for the effect.[8,9] For 3D and 2D cases, magnetoconductance due to weak localization is given by[9]

$$\Delta\sigma_L^{3D}(H,T)=\frac{e^2}{2\pi^2\hbar L_H}f_3(x), \tag{21}$$

$$\Delta\sigma_L^{2D}(H,T)=\frac{e^2}{2\pi^2\hbar}\left[\psi\left(\frac{1}{2}+x\right)-\ln(x)\right], \tag{22}$$

respectively, where $x=L_H^2/4L_{Th}^2\cong 4T^3/H$, $L_H=(\hbar c/eH)^{1/2}$ is the field-dependent dephasing length, ψ is the digamma function, and $f_3(x)$ is given in Ref. 9. The asymptotic form of Eq. (22) is of interest for comparison with the experimental data. At the high-field and low-temperature limit, it is given by

$$\Delta\sigma_L^{2D}(H,T)\propto\ln(H) \quad \text{for} \quad \frac{4T^3}{H}\ll 1, \tag{23}$$

which is temperature independent.[8,9]

For the Coulomb interaction effect, the Zeeman spin splitting effect gives rise to a negative magnetoconductance.[8,9] In a 3D case,[9]

$$\Delta\sigma_I^{3D}(H,T)=-\frac{e^2F}{4\pi^2\hbar}\sqrt{\frac{k_BT}{2\hbar D}}g_3(h), \tag{24}$$

where $h=g\mu_BH/k_BT\cong 1.34H/T$ and

$$g_3(h)=\begin{cases}\sqrt{h}-1.3 & \text{for} \quad \dfrac{H}{T}\gg 1\\[2ex] 0.053h^2 & \text{for} \quad \dfrac{H}{T}\ll 1.\end{cases}$$

Thus the asymptote of Eq. (24) in the same limit as for Eq. (23) is

$$\Delta\sigma_I^{3D}(H,T)=-\frac{e^2F}{4\pi^2\hbar}\sqrt{\frac{g\mu_B}{2\hbar D}}H^{1/2}+\frac{1.3e^2F}{4\pi^2\hbar}\sqrt{\frac{k_BT}{2\hbar D}} \quad \text{for} \quad \frac{H}{T}\gg 1. \tag{25}$$

Therefore, at low temperatures and high fields, Eq. (19) has an asymptotic behavior [from Eqs. (23) and (25)]

$$\Delta\sigma(H,T)=C_1\ln(H)-C_2H^{1/2}+C_3T^{1/2}. \tag{26}$$

Although the experimental conditions ($T=2$–40 K, $H=0$–7.5 T) do not match the asymptotic limit for Eqs. (23) and (25), we can still use Eq. (26) for a qualitative comparison with the experimental data. Apparently, the observed negative magnetoconductance of these samples at low tem-

peratures is due to a dominant interaction effect [the second and third terms of Eq. (26)]. Thus, with decreasing temperature, the magnetoconductance given by Eq. (26) will become increasingly negative. This is exactly what we see in the experimental data (Fig. 7). At higher temperatures, the magnetoconductance becomes positive, suggesting a change of the dominance from the interaction effect at low temperatures to the localization effect at higher temperatures. This change of dominance will be further reinforced by a crossover of the dimensionality of the localization effect from two to three dimensions with increasing temperature. However, it is noted that the observed magnetoconductance changes sign ($\sim$30 K) below the dimensional transition temperature T_s $\sim$60 K (Sec. III A 3). The explanation of this occurrence is that such a dimensional crossover is not an abrupt transition, but rather a gradual one. Near the crossover region, both dimensions contribute to the observed magnetoconductance and it is the interplay between the two that determines where it changes its sign.

C. Thermoelectric power

Thermoelectric power due to free electrons is given by[28]

$$S(T) = -\frac{\pi^2 k_B^2 T}{3e}\left[\frac{d\ln\sigma(E)}{dE}\right]_{E_F}. \tag{27}$$

For metals, a linearly temperature-dependent thermopower $S(T) \propto T$ is a well known property.[28] For a semiconductor with a small band gap, the thermopower is proportional to $1/T$.[28] Figure 8 shows the thermopower results $S(T)$ of these three implanted polymers as a function of temperature. Apparently, these implanted polymers have almost identical thermopower results.

As one can see from Fig. 8(a), the higher-temperature thermopower data follow $S(T) \propto T$ behavior. This linearly T-dependent thermopower is consistent with the conductivity and magnetoconductance results in exhibiting a metallic behavior of these carbonized systems. However, the low-temperature thermopower data increase with decreasing temperature and follow $S(T) \propto 1/T$ [Fig. 8(b)]. Thus the thermopower of these implanted polymers can be described by

$$S(T) = b_1 T + \frac{b_2}{T}, \tag{28}$$

where fitting parameters $b_1 \cong 6.73 \times 10^{-3}\,\mu$V/K and $b_2 \cong 29.6\,\mu$V are obtained for the three implanted samples. There are two possible contributions to the increase of the thermopower at low temperatures. One is the phonon drag effect, observed frequently in metals.[28] However, this effect only causes a ''bump'' in the low-temperature thermopower, which still goes to zero as the temperature is further decreased. The more probable contribution is from the enhanced Coulomb interaction effect at low temperatures due to a reduction of the dimensionality of the localization effect as seen in the magnetoconductance results. It has been shown that the long-range electron-electron interaction effect causes a depletion in the density of states at the Fermi level.[11] Such a depletion in an insulating system will result in a ''Coulomb gap'' effect.[11,29] For example, this effect was used to explain a similar observed thermopower result in palladium film samples near an insulator-metal transition.[30]

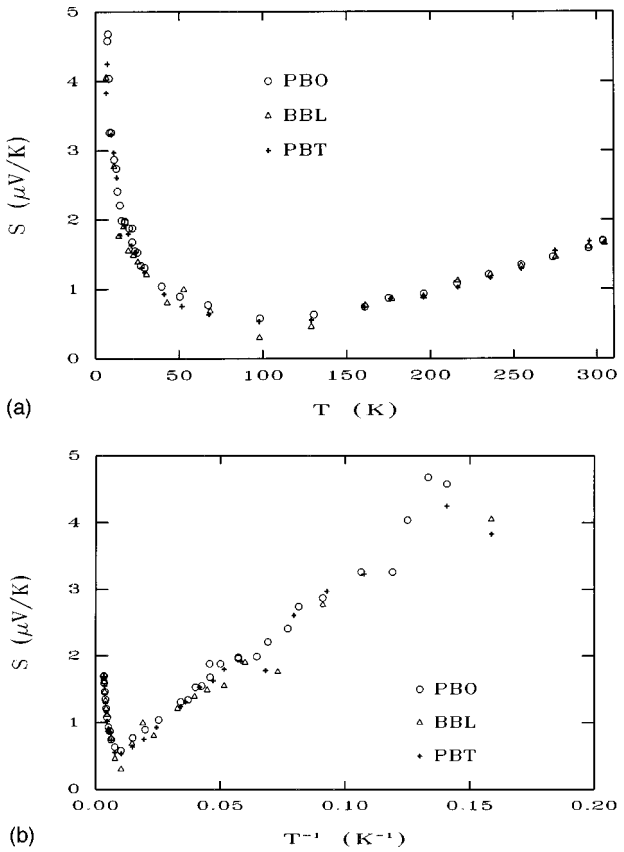

FIG. 8. (a) Thermoelectric power data versus temperature of the implanted PBO, PBT, and BBL. (b) Thermoelectric power data versus $1/T$.

D. Microwave dielectric constant

Dielectric response is another useful experimental tool for probing the transport properties of a conducting material. Figure 9 plots the microwave dielectric constant results of the implanted PBO and BBL. The two results have a similar temperature dependence, but with a somewhat larger difference in magnitude as compared to that between the conductivity and thermopower results of the two samples. This difference is due to a larger measurement uncertainty of the cavity technique. The dielectric constant result calculated

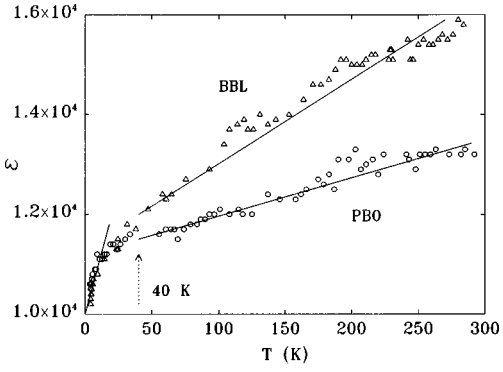

FIG. 9. Microwave frequency (6.5 GHz) dielectric constant results of the implanted PBO and BBL.

from the experimental parameters (shifts in the resonance frequency and Q) is very sensitive to the sample dimensions: A small difference in dimensions can result in a significant deviation in the final result.[14] This experiment also has a larger noise-to-signal ratio that results in a more scattered data curve as one can see in Fig. 9.

Even with a larger measurement error, it can be seen that the dielectric constant results of the implanted polymers are large ($>10^4$) over the whole temperature range. Previous dielectric response studies on doped and highly conducting polymers have shown that they have large positive dielectric constants (up to 10^4).[12,31,32] For a truly metallic system including metallic conducting polymers, the dielectric constant is negative at this frequency.[32,33] Therefore, the large dielectric constants of these implanted materials are also consistent with the semimetallic model.

The observed dielectric constants of implanted PBO and BBL share a similar temperature dependence. At temperatures above ~ 40 K, both sets of data are weakly temperature dependent and at lower temperatures, both results decrease with decreasing temperature more rapidly, as schematically illustrated by the straight lines in Fig. 9. The dielectric constant of a localized system has been found to follow[31,32]

$$\varepsilon \propto N(E_F) L_{loc}^2, \tag{29}$$

where $N(E_F)$ is the density of states at the Fermi level and L_{loc} is the relevant localization length. The slow increase in $\varepsilon(T)$ with increasing temperature at higher temperatures (>40 K) is likely a result of the phonon assisted electron delocalization effect increasing L_{loc}.[32] The more rapid decrease in $\varepsilon(T)$ at lower temperatures indicates other factors taking effect in this temperature region. It is very suggestive to relate this more rapid decrease in the dielectric constant with the enhanced electron-electron interaction effect at low temperatures since the effect of this enhancement is a depletion in the density of states at the Fermi level, which explains the drop in $\varepsilon(T)$ at low temperatures following Eq. (29).

IV. CONCLUSION

In sum, this comprehensive experimental study of the high-dosage ion implanted PBO, PBT, and BBL polymers reveals that these carbonized systems are semimetallic with an unusual low-temperature phase. The conductivity, magnetoconductance, thermopower, and microwave dielectric constants results consistently conclude that these implanted polymers are on the metallic side of an insulator-metal transition. The weakly temperature-dependent conductivity data fit best to a semimetallic model with an electron-electron interaction and weak localization effects dominating the charge transport. This model shows that the electron-electron interaction contribution is 3D over the whole experimental temperature range, while the weak localization effect changes its three to two dimensions with decreasing temperature at $T_s \sim 60$ K. The parameters obtained from the fitting of the conductivity data are within the theoretical predictions concerning the dimensionalities of the two effects. An enhanced interaction effect due to this reduced dimensionality of the localization effect showed systematically in the magnetoconductance, thermopower, and dielectric constant results at low temperatures. The persistence of the interaction effect up to room temperature is explained by a less screened free-electron gas in these highly disordered systems. This conclusion is also consistent with the fitting of $p=3$ from the conductivity results, which indicates dominant electron-phonon scattering in these systems. The conduction charge carriers in these implanted systems arise from unsaturated sp^2 bonds in a 3D interconnected carbon network reformed after ion implantation. The difference between these polymers and the earlier studied ones[2,3] is the pristine structure of these rigid-rod and ladder polymers that provides a compact carbon backbone as a foundation for the reformed carbon network.

ACKNOWLEDGMENTS

This work was supported in part by Air Force OSR Grant No. F49620-92-C0002, the National Science Foundation Grant No. DMR-9508723, and the Office of Naval Research.

*Present address: Air Force Research Lab/MLBP, Wright-Patterson Air Force Base, OH 45433.

†Present address: Department of Chemistry, Kent State University-Stark Campus, 6000 Frank Avenue, Canton, OH 44720.

‡Present address: Department of Physics, Korea University, Seoul 136-701, Korea.

[1] T. Venkatesan, L. Calcagno, B. S. Elman, and G. Foti, in *Ion Beam Modification of Insulators*, edited by P. Mazzoldi and G. W. Arnold (Elsevier, Amsterdam, 1987), p. 301.

[2] M. S. Dresselhaus and R. Kalish, *Ion Implantation in Diamond, Graphite, and Related Materials* (Springer-Verlag, Berlin, 1992), Vol. 22; J. W. Mayer , L. Eriksson, and J. A. Davies, *Ion Implantation of Semiconductors, Silicon and Germanium* (Academic, New York, 1970); G. Carter and W. A. Grant, *Ion Implantation of Semiconductors* (Arnold, London, 1976).

[3] M. L. Kaplan, S. R. Forrest, P. H. Schmidt, and T. Venkatesan, J. Appl. Phys. **55**, 732 (1984).

[4] B. S. Elman, D. J. Sandman, and M. A. Newkirk, Appl. Phys. Lett. **46**, 100 (1985).

[5] B. S. Elman, M. S. Dresselhaus, G. Dresselhaus, E. W. Maby, and H. Mazurek, Phys. Rev. B **24**, 1027 (1981).

[6] A. Burns, Z. H. Wang, G. Du, J. Joo, J. A. Osaheni, S. A. Jenekhe, C. S. Wang, and A. J. Epstein, in *Electrical, Optical, and Magnetic Properties of Organic Solid State Materials*, edited by L. Y. Chiang, A. F. Garito, and D. J. Sandman (Materials Research Society, Pittsburgh, 1992), Vol. 247, p. 735.

[7] J. Robertson, Adv. Phys. **35**, 317 (1986); J. Robertson and E. P. O'Reilly, Phys. Rev. B **35**, 2946 (1987).

[8] S. Kobayashi and F. Komori, Prog. Theor. Phys. Suppl. **84**, 224 (1985).

[9] B. L. Altshuler and A. G. Aronov, in *Electron-Electron Interactions in Disordered Systems*, edited by A. L. Efros and M. Pollak (North-Holland, Amsterdam, 1985), p. 1; P. A. Lee and T. V. Ramakrishnan, Rev. Mod. Phys. **57**, 287 (1985).

[10] In a follow-up paper, we present results of lower dosage im-

planted PBO samples, which show an insulating behavior rather than the semimetallic behavior of these higher dosage samples. G. Du *et al.* (unpublished).

[11] A. L. Efros and B. I. Shklovskii, J. Phys. C **8**, L49 (1975); B. I. Sjklovskii and A. L. Efros, in *Electronic Properties of Doped Semiconductors*, edited by M. Cardona *et al.* (Springer-Verlag, Berlin, 1984), p. 210.

[12] H. H. S. Javadi, A. Chakraborty, C. Li, N. Theophilou, D. B. Swanson, A. G. MacDiarmid, and A. J. Epstein, Phys. Rev. B **43**, 2183 (1991).

[13] S. A. Jenekhe and P. O. Johnson, Macromolecules **23**, 4419 (1990); S. A. Jenekhe and S. J. Tibbetts, J. Polym. Sci., Part B: Polym. Phys. **26**, 201 (1988); J. F. Wolfe and F. E. Arnold, Macromolecules **14**, 909 (1981).

[14] L. Buravov and I. F. Shchegolev, Prib. Tekh. Éksp. **2**, 171 (1971) [Instrum. Exp. Tech. **14**, 528 (1971)].

[15] P. M. Chaikin and J. F. Kwak, Rev. Sci. Instrum. **46**, 218 (1975).

[16] A. G. Zabrodskii and K. N. Zinov'eva, Sov. Phys. JETP **59**, 425 (1984).

[17] N. F. Mott and E. Davis, *Electronic Processes in Non-Crystalline Materials* (Clarendon, Oxford, 1979).

[18] G. A. Thomas, A. Kawabata, Y. Ootuka, S. Katsumoto, S. Kobayashi, and W. Sasaki, Phys. Rev. B **26**, 2113 (1982).

[19] R. F. Milligan, T. F. Rosenbaum, R. N. Bhatt, and G. A. Thomas, in *Electron-Electron Interactions in Disordered Systems* (Ref. 9), p. 231.

[20] G. Bergmann, Phys. Rep. **107**, 1 (1984).

[21] The second term is from the electron-electron interaction effect (Ref. 9). The third term of this function, valid for the whole temperature range, follows the consideration of the first-order localization correction (Ref. 9) for a conducting layer with finite thickness d_c,

$$\Delta\sigma_{WL}=\frac{2e^2}{\pi\hbar}\sum_{q_\perp=0,\pm 2\pi/d_c,\ldots}\int\frac{d^2\mathbf{q}_\parallel}{(2\pi)^2}\frac{1}{q_\perp^2+\mathbf{q}_\parallel^2+1/L_{Th}^2},$$

where $L_{th}^2=D\tau_{in}(T)$ and is in the form $d_c^2(T_s/T)^p$. Evaluating the summation of the given integral, one obtains the third term of Eq. (9).

[22] A. Möbius, J. Phys. C **18**, 4639 (1985).

[23] K. C. Mui, P. Lindenfeld, and W. L. McLean, Phys. Rev. B **30**, R2951 (1984).

[24] J. Stein and U. Krey, Z. Phys. B **37**, 13 (1980).

[25] H. H. Song and C. S. Wang, Polymer **34**, 4793 (1993).

[26] H. H. Song, A. V. Fratini, M. Chabinyc, G. E. Price, A. K. Agrawal, C. S. Wang, D. S. Dudis, and F. E. Arnold, Synth. Met. **69**, 533 (1995).

[27] M. A. Howson and D. Grieg, Phys. Rev. B **30**, 4805 (1984).

[28] R. G. Chambers, *Electrons in Metal and Semiconductors* (Chapman and Hall, London, 1990).

[29] I. S. Shlimak, in *Hopping and Related Phenomena*, edited by H. Fritzsche and M. Pollak (World Scientific, Singapore, 1990), p. 49; P. Dai, Y. Zhang, and M. P. Sarachik, Phys. Rev. Lett. **69**, 1804 (1992).

[30] M. J. Burns, W. C. McCinnis, R. W. Simon, G. Deutscher, and P. M. Chaikin, Phys. Rev. Lett. **47**, 1620 (1981).

[31] Z. H. Wang, H. H. S. Javadi, A. Ray, A. G. MacDiarmid, and A. J. Epstein, Phys. Rev. B **42**, 5411 (1990).

[32] J. Joo, Z. Oblakowshi, G. Du, J. P. Pouget, E. J. Oh, J. M. Wiesinger, G. Min, A. G. MacDiarmid, and A. J. Epstein, Phys. Rev. B **49**, 2977 (1994); J. Joo, G. Du, V. N. Prigodin, J. Tsukamoto, and A. J. Epstein, *ibid.* **52**, 8060 (1995); R. Kohlman, J. Joo, Y. Z. Wang, J. P. Pouget, H. Kaneko, T. Ishiguro, and A. J. Epstein, Phys. Rev. Lett. **74**, 773 (1995).

[33] G. Burns, *Solid State Physics* (Academic, New York, 1985).